

Tunneling Spin Injection into Single Layer Graphene

Wei Han, K. Pi, K. M. McCreary, Yan Li, Jared J. I. Wong, A. G. Swartz, and R. K. Kawakami[†]

Department of Physics and Astronomy, University of California, Riverside, CA 92521

[†] e-mail: roland.kawakami@ucr.edu

Abstract:

We achieve tunneling spin injection from Co into single layer graphene (SLG) using TiO₂ seeded MgO barriers. A non-local magnetoresistance (ΔR_{NL}) of 130 Ω is observed at room temperature, which is the largest value observed in any material. Investigating ΔR_{NL} vs. SLG conductivity from the transparent to the tunneling contact regimes demonstrates the contrasting behaviors predicted by the drift-diffusion theory of spin transport. Furthermore, tunnel barriers reduce the contact-induced spin relaxation and are therefore important for future investigations of spin relaxation in graphene.

PACS numbers: 85.75.-d, 81.05.ue, 73.40.Gk, 72.25.Hg

Spintronics utilizes the electron's spin degree of freedom in addition to its charge in electronic devices for advanced approaches to information storage and processing [1]. Single layer graphene (SLG) is a promising material for spintronics due to the low intrinsic spin-orbit and hyperfine couplings [2], long spin diffusion lengths ($\sim 2 \mu\text{m}$) [3], and predictions of fascinating spin dependent behavior [4, 5]. Furthermore, SLG is the first material to achieve gate tunable spin transport at room temperature [3, 6, 7]. However, to realize its full potential for spintronics, there are two critical challenges. First, the measured spin lifetimes in SLG (50-200 ps) are orders of magnitude shorter than expected from the intrinsic spin-orbit coupling [2, 3, 8-11]. Consequently, substantial theoretical and experimental effort is focused on identifying the extrinsic mechanism of spin scattering [9, 11, 12]. The second important challenge is to achieve tunneling spin injection into SLG. This will produce efficient spin injection by overcoming the conductance mismatch between the ferromagnetic (FM) metal electrodes and the SLG [13-15]. Up to now, enhancing the spin injection efficiency has focused on reducing the conductance mismatch by decreasing the contact area using MgO masking layers or barriers with pinholes [7, 8, 10, 16-18]. However, tunneling spin injection has not been achieved due to the difficulty to growing uniform, pinhole-free tunnel barriers on graphene.

In this Letter, we demonstrate tunneling spin injection in SLG spin valves and report large spin signals and enhanced spin lifetimes. Using TiO_2 seeded MgO films as the tunnel barrier, we observe a non-local magnetoresistance (ΔR_{NL}) as high as 130Ω at room temperature, which is the largest value observed in any material. The I - V characteristics of the contact resistance are highly non-linear and ΔR_{NL} varies inversely with the SLG conductivity, which are the two principal characteristics of tunneling spin injection. Furthermore, the spin lifetimes (450-500 ps) are considerably longer than previously observed for transparent and pinhole contacts (50-200 ps)

[3, 8-10], which suggests that the tunnel barrier greatly reduces the contact-induced spin relaxation. These results are important for applications such as spin-based logic [19] and for fundamental studies of spin relaxation in graphene.

Graphene spin valves are fabricated using mechanically exfoliated SLG flakes on SiO₂/Si substrate, where the Si is used as a back gate. Co electrodes are defined by electron-beam lithography using PMMA/MMA bilayer resist to produce undercut, followed by angle evaporation in a molecular beam epitaxy system with a base pressure of 2×10^{-10} torr. Tunneling contacts are fabricated in the following manner. First, 0.12 nm of Ti is deposited at both 0° and 9° angles (Figure 1a), followed by oxidation in 5×10^{-8} torr of O₂ for 30 minutes to convert the metallic Ti into insulating TiO₂. The presence of TiO₂ greatly improves the uniformity of MgO overlayers [20]. A 3 nm MgO masking layer is deposited at an angle of 0° and a 0.8 nm MgO tunnel barrier is deposited at an angle of 9°. Then the 80 nm thick Co electrode is deposited with an angle of 7°. Figure 1b illustrates the geometry of the tunneling contact, where the current flows across the 0.8 nm MgO tunnel barrier of width ~50 nm. Approximately 20% of the tunneling electrodes possess pinholes, which are utilized for investigating the characteristics of spin injection through pinhole contacts. For the transparent contacts, the Co is directly contacted to SLG with a 2 nm MgO masking layer [7, 8].

Spin injection and transport are measured on samples held at 300 K in helium atmosphere using the non-local geometry with standard ac lock-in techniques [3, 21]. The inset of Figure 1c shows the non-local measurement where the spin is injected at electrode E2 and detected at E3. The non-local resistance, R_{NL} , is defined as the measured voltage signal (V_{NL}) divided by the injection current (I). Figure 1c shows R_{NL} as the magnetic field is swept up (black curve) and swept down (red curve) for a device with tunneling contacts. ΔR_{NL} is defined as the difference of

R_{NL} between the parallel and antiparallel magnetization states of E2 and E3. For spin transport across the 2.1 μm electrode gap (L), ΔR_{NL} is 130 Ω (Figure 1c), which is the largest value observed in any lateral spin valve including metals and semiconductors [3, 6] [7, 16, 22]. For tunneling contacts [3]

$$\Delta R_{NL} = \frac{1}{\sigma_G} \frac{P_J^2 \lambda_G}{W} e^{-L/\lambda_G} \quad (1)$$

where P_J is the spin injection/detection efficiency, and σ_G , W , and λ_G are the conductivity, width, and spin diffusion length of the SLG, respectively. P_J is calculated to be 26-30% using experimental values of $\sigma_G = 0.35 \text{ mS}$, $W = 2.2 \mu\text{m}$, $L = 2.1 \mu\text{m}$, and typical values of $\lambda_G = 2.5\text{-}3.0 \mu\text{m}$ (see Figure 4). This compares favorably with the tunneling spin polarization of 35% measured by spin-dependent tunneling from Co into a superconductor across polycrystalline Al_2O_3 barriers [23]. The spin injection efficiency is larger than observed in previous studies using barriers with pinholes (2% – 18% at low bias) [3, 10, 16] and transparent contacts (1%) [8].

The tunnel barrier enhances the efficiency of spin injection from Co into the SLG by alleviating the conductance mismatch problem [13-15]. For spin injection without tunnel barriers, the spins that are injected from the Co electrode into the SLG can diffuse within the SLG (toward neighboring electrodes) or diffuse back into the Co electrode. The flow of spin via diffusion is governed by the spin resistances [18] which are $R_G = \lambda_G / (\sigma_G W)$ for the SLG, and $R_F = \rho_F \lambda_F / A_J$ for the Co, where ρ_F is the Co resistivity, λ_F is the spin diffusion length of Co, and A_J is the junction area [24]. Using typical parameters ($W = 2 \mu\text{m}$, $\lambda_G = 2\text{-}3 \mu\text{m}$, $\sigma_G = 0.5 \text{ mS}$, $\rho_F = 6 \times 10^{-8} \Omega \text{ m}$ [25], $\lambda_F = 0.06 \mu\text{m}$ [26]), the R_F/R_G ratio has values between $\sim 10^{-3}$ and $\sim 10^{-5}$ depending on the value of A_J [24]. Because $R_F \ll R_G$, the spin diffusion is dominated by the back flow of spins into the Co electrode, which leads to a low spin injection efficiency. The

insertion of a tunnel barrier increases the spin injection efficiency by blocking the back flow of spins into the Co electrode.

Quantitatively, the role of the tunnel barrier is explained in the one-dimensional drift-diffusion theory of spin transport [18], where ΔR_{NL} is given by

$$\Delta R_{NL} = 4R_G e^{-L/\lambda_G} \left(\frac{P_J \frac{R_J}{R_G}}{1 - P_J^2} + \frac{P_F \frac{R_F}{R_G}}{1 - P_F^2} \right)^2 \times \left(\left(1 + \frac{2 \frac{R_J}{R_G}}{1 - P_J^2} + \frac{2 \frac{R_F}{R_G}}{1 - P_F^2} \right)^2 - e^{-2L/\lambda_G} \right)^{-1} \quad (2)$$

where P_F is the spin polarization of the FM and R_J is the contact resistance between the FM and SLG. This equation shows that increasing the contact resistance produces a strong enhancement of ΔR_{NL} that saturates as R_J becomes significantly larger than R_G [see supplemental information]. In addition to the magnitude of ΔR_{NL} , another method to distinguish the tunneling contacts is to investigate the relationship between ΔR_{NL} and σ_G , which can be tuned by gate voltage. For tunneling contacts ΔR_{NL} scales with $1/\sigma_G$ (equation 1), while for transparent contacts ($R_J \ll R_G$) ΔR_{NL} scales with σ_G [7, 11]. Figure 2 shows the calculated gate dependence of ΔR_{NL} for transparent, intermediate ($R_J \sim R_G$), and tunneling contacts [see supplemental information]. For transparent contacts, the linear increase of ΔR_{NL} with gate voltage is due to the linear increase of σ_G away from the Dirac point [27]. For tunneling contacts, ΔR_{NL} varies inversely with gate voltage and exhibits a peak at the Dirac point.

Figures 3a and 3b show the experimental results for the gate dependence of ΔR_{NL} for SLG spin valves with transparent and pinhole contacts, respectively. The I - V characteristic of the contact resistance is determined by a three-probe lock-in measurement (current is applied across E1 and E2, voltage measured across E3 and E2). For both cases, the nearly constant bias dependence of $(dV/dI)_C$ (insets of Figures 3a and 3b) corresponds to a nearly linear I - V

characteristic. For transparent contacts, ΔR_{NL} (black squares) exhibits a minimum at the Dirac point, and a linear relationship with σ_G (red curve), which verifies the theoretical prediction (Figure 2, top curve). For pinhole contacts, ΔR_{NL} (black squares) shows relatively little variation and has a weak minimum near the Dirac point which is similar to the case of intermediate contact resistance as calculated in Figure 2 (middle curve). For both the transparent and pinhole contacts, the non-local MR and I - V characteristics are consistent with previous studies [3, 7, 8, 10, 16] which exhibit a minimum in ΔR_{NL} at the Dirac point and nearly linear I-V curves for the contacts.

For tunneling contacts, the $(dI/dV)_C$ is highly non-linear (Figure 3c inset) and exhibits little temperature dependence, which are consistent with tunneling transport across the Co/MgO/TiO₂/SLG junctions. Figure 3c shows the gate dependence of ΔR_{NL} (black squares) and σ_G (red curve) for tunneling contacts. Interestingly, ΔR_{NL} exhibits a maximum at $V_g = 2$ V near the Dirac point, which is the first time this has been observed experimentally. The origin of the asymmetry of ΔR_{NL} vs. V_g is unclear and varies from sample to sample. The observed peak structure in the gate dependence is a key characteristic of tunneling spin injection (Figure 2, bottom curve), and has been reproduced on four different devices. This inverse scaling of ΔR_{NL} with σ_G is associated with the spin injection process as opposed to spin detection. Specifically, spin injection produces a difference in the spin-dependent chemical potential at the tunnel barrier/SLG interface given by $\Delta\mu = \mu_\uparrow - \mu_\downarrow = eP_JR_GI$ [18]. Thus, a larger R_G will increase ΔR_{NL} due to a greater difference in the spin-dependent chemical potential.

While the achievement of tunneling spin injection will be important for applications in spintronics, it will also have a strong impact on fundamental studies of spin relaxation in graphene. As shown in Figures 4a and 4b, the spin lifetimes measured at the Dirac point are 495

ps and 448 ps for tunneling SLG spin valves with 2.1 μm and 5.5 μm spacing, respectively. These are much longer than the spin lifetimes of 134 ps for pinhole contacts (Figure 4c) and 84 ps for transparent contacts (Figure 4d), which are consistent with the values reported in previous studies (50 - 200 ps) [3, 8-10]. The spin lifetimes are obtained by applying an out-of-plane magnetic field (H_{\perp}) to induce spin precession and fitting the resulting Hanle curves (see [11] for details) with

$$R_{NL} \propto \pm \int_0^{\infty} \frac{1}{\sqrt{4\pi Dt}} \exp\left[-\frac{L^2}{4Dt}\right] \cos(\omega_L t) \exp(-t/\tau_s) dt \quad (3)$$

where the + (-) sign is for the parallel (antiparallel) magnetization state, D is the diffusion constant, τ_s is the spin lifetime, and $\omega_L = g\mu_B H_{\perp}/\hbar$ is the Larmor frequency. Theoretically, the measured spin lifetime (τ_s) is determined by the spin-flip scattering within the SLG (at a rate of τ_{sf}^{-1}) and spin relaxation induced by the Co contacts. In the latter effect, the spins diffuse into the Co contact with characteristic escape time (τ_{esc}), which limits the measured spin lifetime. For $\lambda_G \rightarrow \infty$, these time scales are simply related by $\tau_s^{-1} = \tau_{sf}^{-1} + \tau_{esc}^{-1}$ [28], while for the more realistic case of finite λ_G , the influence of the contact-induced relaxation should be reduced. Furthermore, spin-flip scattering at the Co/SLG interface may introduce additional spin relaxation. Due to the increased spin lifetimes, the spin diffusion lengths from the Hanle fits ($\lambda_G = \sqrt{D\tau_s}$) are significantly larger for tunneling contacts (2.5-3.0 μm) than for transparent and pinhole contacts (1.2-1.4 μm). The longer spin lifetimes and spin diffusion lengths with tunneling contacts indicate that the effect of the contact-induced relaxation is substantial for transparent and pinhole contacts. Thus, tunnel barriers reduce the contact-induced relaxation and enable a more accurate measurement of τ_{sf} for fundamental studies of spin relaxation.

In conclusion, we have successfully achieved tunneling spin injection into SLG using TiO₂

seeded MgO barriers and observe enhanced spin injection efficiencies and large ΔR_{NL} . Investigating ΔR_{NL} vs. σ_G for the different contact regimes (from transparent to tunneling) realizes the contrasting behaviors predicted by the drift-diffusion theory. Finally, tunnel barriers reduce the contact-induced spin relaxation and are therefore important for future investigations of spin relaxation in graphene.

We acknowledge stimulating discussions with E. Johnston-Halperin and acknowledge the support of ONR (N00014-09-1-0117), NSF (CAREER DMR-0450037), and NSF (MRSEC DMR-0820414).

References:

- [1] S. A. Wolf *et al.*, Science **294**, 1488 (2001).
- [2] D. Huertas-Hernando, F. Guinea, and A. Brataas, Phys. Rev. B **74**, 155426 (2006).
- [3] N. Tombros *et al.*, Nature **448**, 571 (2007).
- [4] Y.-W. Son, M. L. Cohen, and S. G. Louie, Nature **444**, 347 (2006).
- [5] W. Y. Kim, and K. S. Kim, Nature Nanotech. **3**, 408 (2008).
- [6] S. Cho, Y.-F. Chen, and M. S. Fuhrer, Appl. Phys. Lett. **91**, 123105 (2007).
- [7] W. Han *et al.*, Phys. Rev. Lett. **102**, 137205 (2009).
- [8] W. Han *et al.*, Appl. Phys. Lett. **94**, 222109 (2009).
- [9] C. Jozsa *et al.*, Phys. Rev. B **80**, 241403(R) (2009).
- [10] M. Popinciuc *et al.*, Phys. Rev. B **80**, 214427 (2009).
- [11] K. Pi *et al.*, Phys. Rev. Lett. **104**, 187201 (2010).
- [12] A. H. Castro Neto, and F. Guinea, Phys. Rev. Lett. **103**, 026804 (2009); D. Huertas-Hernando, F. Guinea, and A. Brataas, Phys. Rev. Lett. **103**, 146801 (2009); C. Ertler et al., Phys. Rev. B **80**, 041405(R) (2009).

- [13] G. Schmidt *et al.*, Phys. Rev. B **62**, 4790(R) (2000).
- [14] E. I. Rashba, Phys. Rev. B **62**, 16267(R) (2000).
- [15] A. Fert, and H. Jaffres, Phys. Rev. B **64**, 184420 (2001).
- [16] C. Jozsa *et al.*, Phys. Rev. B **79**, 081402(R) (2009).
- [17] T. Kimura, Y. Otani, and J. Hamrle, Phys. Rev. B **73**, 132405 (2006).
- [18] S. Takahashi, and S. Maekawa, Phys. Rev. B **67**, 052409 (2003).
- [19] H. Dery *et al.*, Nature **447**, 573 (2007).
- [20] W. H. Wang *et al.*, Appl. Phys. Lett. **93**, 183107 (2008).
- [21] M. Johnson, and R. H. Silsbee, Phys. Rev. Lett. **55**, 1790 (1985).
- [22] T. Kimura, and Y. Otani, Phys. Rev. Lett. **99**, 196604 (2007); X. Lou et al., Nature Phys. **3**, 197 (2007); O. M. J. van't Erve et al., Appl. Phys. Lett. **91**, 212109 (2007).
- [23] R. Meservey, and P. M. Tedrow, Phys. Rep. **238**, 173 (1994).
- [24] Because of the ultrathin nature of the SLG, the current density experiences a significant change at the junction. Thus, the effective A_J should have a value between the Co/SLG contact area and $W \times (\text{SLG thickness})$. For the estimation of R_F/R_G , the range is determined using $A_J = W \times 50 \text{ nm}$ and $A_J = W \times (\text{SLG thickness})$.
- [25] D. R. Lide, CRC Handbook of Chem. and Phys., CRC Press, Boca Raton, Florida, USA (1998).
- [26] L. Piraux *et al.*, Eur. Phys. J. B. **4**, 413 (1998).
- [27] A. K. Geim, and K. S. Novoselov, Nature Mater. **6**, 183 (2007).
- [28] M. Zaffalon, and B. J. van Wees, Phys. Rev. B **71**, 125401 (2005).

FIGURE CAPTIONS:

Figure 1: (a) Schematic diagram of the angle evaporation geometry. The grey layers are PMMA/MMA resist with undercut. The red and blue dashed lines show the 0° and 9° deposition of TiO_2 and MgO . The black lines indicate the 7° evaporation of Co. (b) Schematic drawing of the Co/MgO/TiO₂/SLG tunneling contacts. The arrow indicates the current flow through the MgO tunnel barrier. (c) Non-local MR scans of a SLG spin valves measured at room temperature. The black (red) curve shows the non-local resistance as the magnetic field is swept up (down). The non-local MR (ΔR_{NL}) of 130Ω is indicated by the arrow. Inset: the non-local spin transport measurement on this device with a spacing of $L = 2.1 \mu\text{m}$ and SLG width of $W = 2.2 \mu\text{m}$.

Figure 2: Predictions of the drift-diffusion theory of spin transport. The non-local MR as a function of gate voltage for three different types of contacts between Co and SLG: transparent, intermediate, and tunneling. The curves are normalized by their value at zero gate voltage.

Figure 3: (a-c) Non-local MR (black squares) and conductivity (red lines) as a function of gate voltage for SLG spin valves with transparent, pinhole and tunneling contacts, respectively. Inset: the differential resistance of the contact, $(dV/dI)_C$, as a function of bias current.

Figure 4: (a) Hanle spin precession for SLG spin valves with tunneling contacts ($R_J = 30-70 \text{ k}\Omega$, non-linear) for $L=2.1 \mu\text{m}$. (b) Hanle spin precession for tunneling contacts ($R_J = 20-40 \text{ k}\Omega$, non-linear) with $L=5.5 \mu\text{m}$. (c) Hanle spin precession for pinhole contacts ($R_J = 6 \text{ k}\Omega$, linear) with $L=2.0 \mu\text{m}$. (d) Hanle spin precession for transparent contacts ($R_J < 0.3 \text{ k}\Omega$, linear) with $L=3.0 \mu\text{m}$. The top (red/grey) and bottom (black) curves correspond to Hanle curves of the parallel and anti-parallel states, respectively. The solid lines are best fit curves based on equation 3. The units for D are m^2/s .

Figure 1

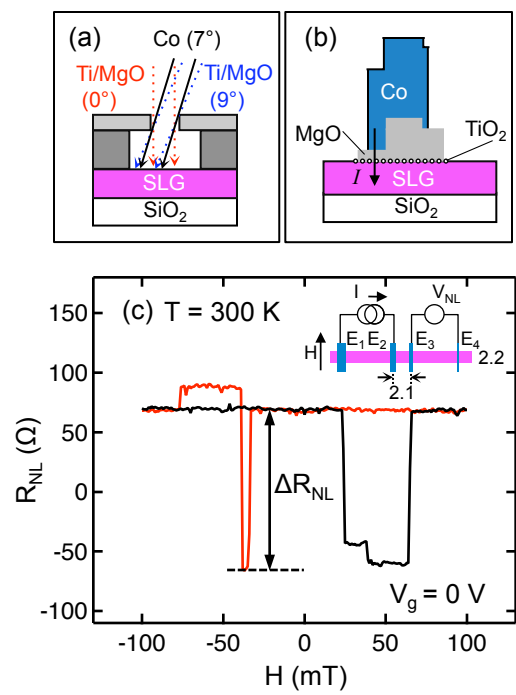


Figure 2

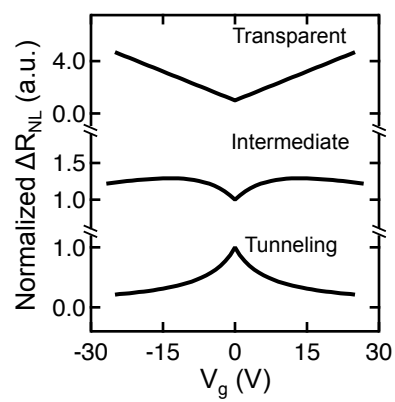


Figure 3

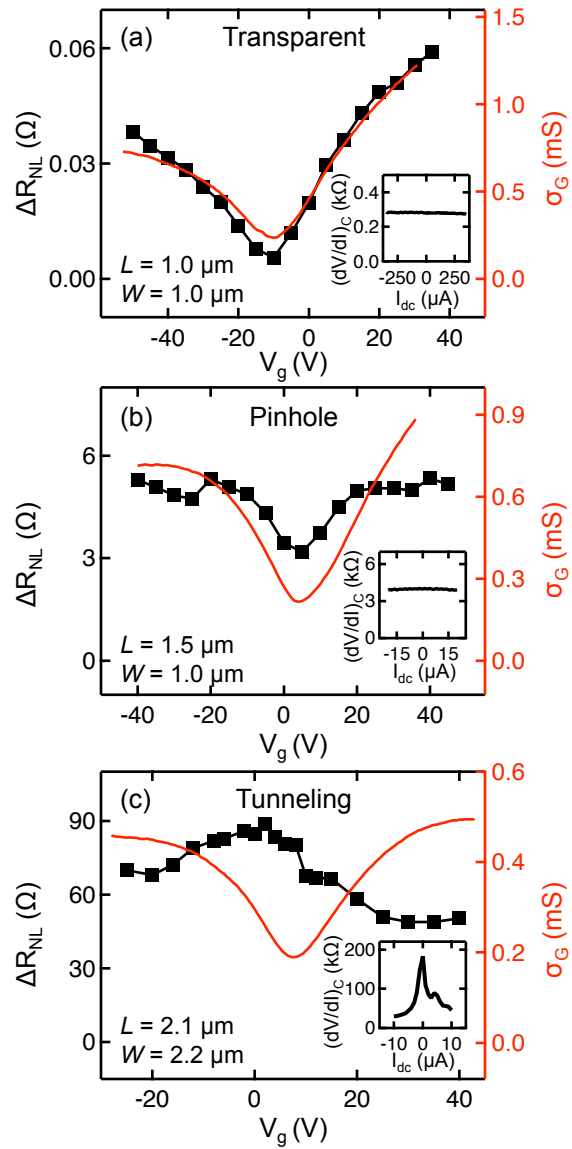


Figure 4

